

Hybrid superinductance with Al/InAs

Junseok Oh,¹ Ido Levy,² Tyler Cowan,² Jacob Issokson,² Archana Kamal,³ Javad Shabani,² and Andrew P. Higginbotham^{1,4}

¹⁾*The James Franck Institute, University of Chicago, Chicago, Illinois 60637, USA*

²⁾*Center for Quantum Phenomena, Department of Physics, New York University, New York 10003, USA*

³⁾*Department of Physics and Astronomy, Northwestern University, Evanston, Illinois 60208, USA*

⁴⁾*The Department of Physics, University of Chicago, Chicago, Illinois 60637, USA*

(Dated: 16 January 2026)

We report microwave spectroscopy of Josephson junctions chains made from an epitaxial Al/InAs heterostructure. The chains exhibit superinductance, with characteristic wave impedance exceeding $R_Q = \hbar/(2e)^2$. The planar nature of the junctions results in a large plasma frequency, with no measurable deviations from ideal dispersion up to 12 GHz. Internal quality factors decrease sharply with frequency, which we describe with a simple loss model. The possibility of a loss mechanism intrinsic to the superconductor-semiconductor junction is considered.

I. INTRODUCTION

Superconducting circuits are currently a topic of interest, driven by the growth of superconducting quantum computing¹. High-impedance circuits, most notably the fluxonium qubit², have appealing properties such as high coherence³, high-fidelity gates^{4,5}, and routes to noise protection^{6–8}. The enabling circuit element for high-impedance qubits is a superinductor – a device whose characteristic impedance Z exceeds the resistance quantum $R_Q = \hbar/4e^2 \approx 1.027 \text{ k}\Omega^9$. Creating ideal superinductance remains challenging because of stringent and often conflicting requirements. Take superinductance realized by a chain of Josephson junctions as an example. In a tunnel junction, avoiding phase slips requires a small charging energy $E_C \ll E_J$ where E_C is the junction charging energy and E_J is the Josephson energy. However small E_C comes at a cost, since it leads to small plasma frequency $\omega_p \sim \sqrt{E_C E_J}$, reducing operating frequencies. Thus, there are conflicting constraints on E_C that must be navigated.

The challenge of creating ideal superinductance has recently motivated exploration of alternative approaches^{10–14}. Superconductor-semiconductor hybrids are an interesting system for consideration. The ability to make gate-tunable, field-resilient, and high-transparency Josephson junctions in this system has already yielded a series of exciting developments in the demonstration of gate-tunable transmon qubits^{15–17}, Andreev qubits^{18,19}, and amplifiers^{20,21}. Recently the first fluxonium hybrid qubit was demonstrated using an Al/InAs array as the inductive element²², posing the new problem of hybrid superinductance.

Hybrid superinductance is radically different from tunnel-junction superinductance. Due to planar geometry, hybrid junctions have a large charging energy; $E_C > E_J$ is nearly unavoidable. While yielding the benefit of high plasma frequency, the presence of a large charging energy immediately raises the potential drawback of quantum phase slips. On the other hand, in hybrid junctions phase slips may be suppressed due to high transparency^{23,24}, which occurs without fine tuning in the diffusive limit²⁵. Does hybrid superinduc-

tance confer the ability to break the superinductance “barrier” $E_C/E_J > 1$, yielding high plasma frequency? Or, rather, is performance degraded by phase slips? The above conundrum motivated our study.

We fabricate chains of Josephson junctions from an Al/InAs 2D electron gas and investigate their microwave response. In order to obtain a sufficiently large inductance without stray capacitance from electrostatic gates, we explore arrays in the long-junction limit²⁶. Comparing devices with different junction sizes, we reach the superinductance regime $Z > R_Q$, and, unlike conventional Al/AlOx devices, find no resolvable limitations from the single-junction plasma frequencies. The observed dispersion is well described by finite-element microwave simulations. Quality factors decrease sharply with increasing mode frequency, which is the opposite of the behavior expected from phase slips. Rather, we find that loss is well described by an effective resistance shunting the junctions. Although the shunt’s microscopic origin is not certain, we suggest that it is related to our use of junctions in the diffusive limit, and discuss mitigation strategies that would make our superinductance approach practical for fluxonium qubits. At current quality levels, our devices are promising for readout of spin^{27–30} and parity qubits^{31–33} at modest frequencies (< 1 GHz), potentially outperforming dominant coil inductors³⁴ by offering higher quality factor, reduced capacitance, and compact form factor.

II. EXPERIMENT AND RESULTS

The devices are on-chip resonators capacitively coupled to a coplanar waveguide in the hanger geometry (Fig. 1(a)). Each resonator consists of 800 planar Al/InAs Josephson junctions in series. The material stack shown in Fig. 1(c) is prepared by epitaxial growth. The mobility and the carrier density of the film was determined with Hall measurement to be $(1.5 \pm 0.2) \times 10^4 \text{ cm}^2/\text{Vs}$ and $9.76 \times 10^{11} \text{ cm}^{-2}$. We use electron-beam lithography to pattern and selective etching to form Al islands, followed by similar steps to form 1 μm -wide pillar-like structure of semiconducting layers, commonly referred to as “mesa.” The Al islands of the resulting devices are

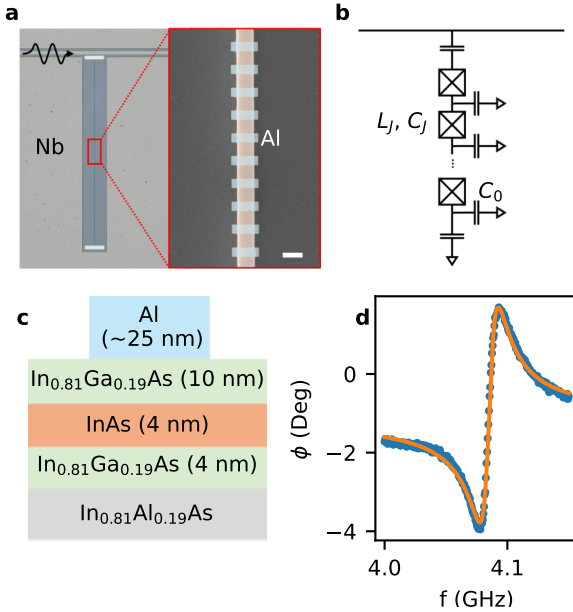


FIG. 1. (a) Left: Optical image of a chain of 800 Josephson junctions is capacitively coupled to a coplanar waveguide (CPW) in the hanger geometry. Right: the close-up image taken with a scanning electron microscope, Al islands (blue) above the InAs 2D electron gas (orange) are separated by the junction length l_J , forming Josephson junction chains. The unit cell size is $d = 1.2 \mu\text{m}$ for all devices. Scale bar on the bottom right is $1 \mu\text{m}$. (b) Lumped element model of a Josephson junction chain. (c) Top layers of the material stack. InGaAs/InAs/InGaAs layers form 2D electron gas. The two capacitors at each end of the chain represents coupling capacitors. (d) S_{21} phase data (points) and the fit (solid line) of the mode 3 of the 700 nm Device 1 at the base temperature.

separated by junction length l_J and unit cell size $d = 1.2 \mu\text{m}$ to form planar Josephson junctions.

Three devices are fabricated and measured: two devices with $l_J = 700 \text{ nm}$ (Device 1,2) and a device with $l_J = 400 \text{ nm}$ (Device 3). The Josephson junction chain can be understood as an equivalent circuit shown in Fig. 1(b). Each Josephson junction has a shunt capacitance C_J , an equivalent inductance L_J given by the Josephson relation, and a parasitic capacitance C_0 to ground. The experimental microwave setup is standard for circuit quantum electrodynamics experiments. Measurements are performed using a vector network analyzer and a dilution refrigerator with a base temperature of 23 mK. The microwave input line is equipped with attenuators for thermalization. On the readout line, a double-junction 4-8 GHz isolator at base temperature is followed by a cryogenic high electron mobility transistor amplifier on the 4 Kelvin stage and a room temperature amplifier.

In Device 1, measured microwave transmission shows a resonance near 4.1 GHz (Fig. 1(d)), yielding resonator parameters $Q_{\text{tot}} = 257$, $Q_{\text{ext}} = 2830$, and $Q_i = 284$ when fit³⁵. The fit Q_{ext} is reasonably close to expectations based on finite-element simulations (4120), indicating that the external coupling is understood.

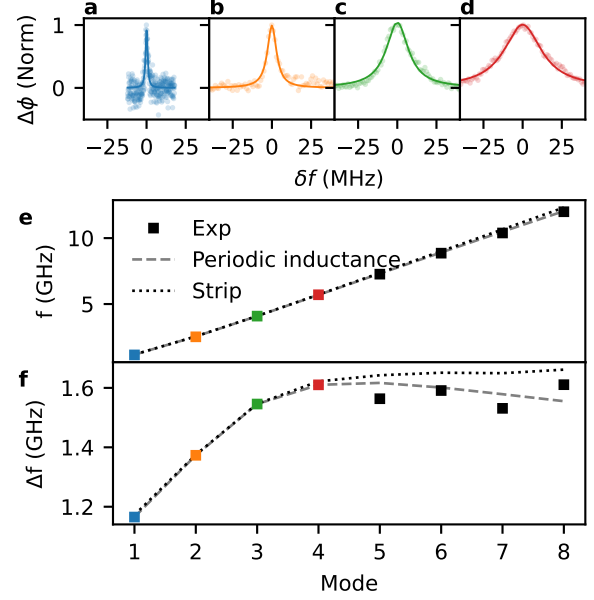


FIG. 2. (a-d) Mode 1 - 4 of Device 1 measured through two-tone spectroscopy. The phase shift $\Delta\phi$ of the mode 3 was measured while a secondary pump was swept through each mode. The pump power was kept sufficiently low to stay in linear regime. The solid lines are fits to Lorentzian. (e) Mode frequencies and (f) mode spacing (Δf) extracted from the fit as a function of mode number. Up to mode 8, the dispersion is nearly linear. The dashed grey line represents the dispersion simulated using an EM solver with 800 unit cells of alternating inductance. The dotted black line is the simulation result for a strip with a uniform inductance.

To identify other modes in a broader frequency range, two-tone spectroscopy was used; while measuring the S_{21} of the resonator at 4 GHz with the vector network analyzer, a secondary pump tone was swept through a wide frequency range. When the pump tone is resonant with j^{th} mode of the resonator, there is a cross-Kerr shift δf_i in the i^{th} mode which can be detected by a vector network analyzer. For all two-tone measurements, δf_3 was measured for Device 1 and 2, and δf_1 for Device 3. Fig. 2(a-d) shows the measured phase shift δf_3 near $j = 3$ mode of the Device 1 while the pump tone is swept through mode 1-4. The pump power was carefully kept low to ensure a “linear response” regime ($\delta f_i = K_{ij}\langle n_j \rangle$), allowing the mode line-shape to be faithfully extracted. Here, K_{ij} is the cross-Kerr coefficient for modes i and j , and $\langle n_j \rangle$ is the average number of photons in mode j ^{36,37}. A Lorentzian fit was applied to the two-tone data to obtain the resonance frequencies and loaded quality factors. We first study the mode frequencies, and then the quality factors.

The extracted mode frequencies and mode spacings of Device 1 are plotted in Fig. 2(e) and (f), respectively. Fig. 2(e) shows a nearly linear dispersion relation up to mode 8. Above mode 8, the Q becomes too small to yield a reliable Lorentzian fit. A more detailed view of the mode dispersion can be gained by examining the mode spacing, $\Delta f_i = f_i - f_{i-1}$ with $f_0 = 0$ (Fig. 2(f)). The mode spacing initially increases up

to mode 4 and decreases above mode 4, showing a slight deviation from the linear dispersion. The initial increase in the mode spacing can be attributed to the coupling capacitors at the end of the chain⁹. To gain quantitative understanding of the mode spacing, we performed finite-element simulations of the device, representing junctions as regions of large sheet inductance and Al as regions with vanishing sheet inductance. A junction inductance of 1.8 nH per unit cell accurately reproduces the measured dispersion (Fig. 2(e-f)). Thus, the slight curvature in the dispersion does not reflect a Josephson plasma frequency – it is a consequence of the electromagnetic environment and device geometry. Combined with the measured speed of light in the chain (mode spacing $\Delta f \approx f_4 - f_3 \approx 1.5$ GHz), we find a chain impedance of 4.7 kOhm, indicating that we have successfully realized an Al/InAs hybrid superinductor. Through the same calculation, C_0 is estimated to be ≈ 80 aF. As shown in Fig. 2(f), a distributed strip inductance shows less dispersion than a periodic inductor, and does not match the experiment as well. We conclude that, while there is no indication of the shunt capacitance affecting dispersion, periodic inductance does play a role.

The same procedure was used to extract dispersion, mode spacing, and inductance for other measured devices (Fig. 3). For the second 700 nm device (Device 2), we find a similar dispersion, Josephson inductance (2.14 nH), and characteristic impedance (5.17 k Ω), compared to Device 1. In contrast, the device with 400 nm junction length exhibits larger mode spacing, lower Josephson inductance (0.11 nH) and lower wave impedance (1.07 k Ω). The drastic difference in inductance between 400 nm and 700 nm junction size is expected based on their relative lengths²⁶. Reproducibility between two devices and control over the dispersion indicates that our devices are well controlled. We notice the 400 nm device shows a larger deviation from the simulation compared to the 700 nm devices, which we attribute to microwave problems specific to that cooldown.

For all devices, the finite element simulation of periodic inductance captures the observed dispersion without any additional junction shunting capacitance. This is consistent with the fact that the C_J is vanishingly small for planar junction. In contrast, standard Al/AlOx superinductance typically has large dispersion^{9,38}, dominated by the Josephson shunt capacitance. The negligible shunt capacitance of planar Al/InAs junctions may therefore open the door to higher-frequency Josephson superinductance.

It is interesting that small C_J makes a nominal criterion for superinductance², $N > \sqrt{C_J/C_0}$, difficult to achieve. The criterion is an assertion that array self-resonant frequencies should be larger than the single-junction plasma frequency. For planar junctions, where the junction plasma frequency is immeasurably large, the criteria is no longer applicable. Rather, one need only ensure that array self-resonances are outside of the band of interest.

The Q values of our Al/InAs superinductors are orders of magnitude smaller than Al/AlOx superinductors⁹. Q_l decreases dramatically with mode frequency, decreasing by an order of magnitude between 1 – 10 GHz, and obeys an ap-

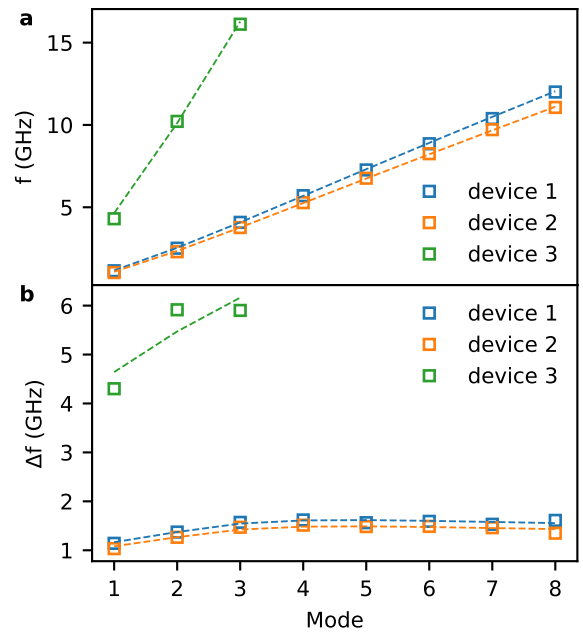


FIG. 3. (a) The mode frequencies and (b) the mode spacing for all measured devices. EM simulation results with periodic inductance are shown in dashed lines.

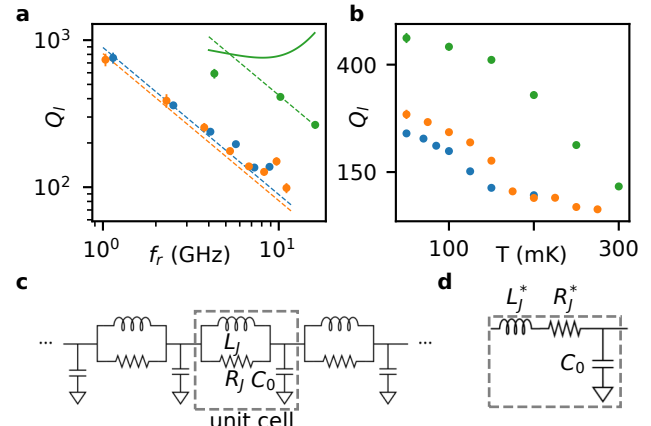


FIG. 4. (a) Q_l as a function of frequency for all devices in log-log scale. Dashed lines represent fits to Eq. 3 assuming $Q_c \gg Q_l$ such that $Q_l \approx Q_c$. For device 3 the simulated Q_c (solid line) approaches Q_l for the lowest-frequency point, which is therefore excluded from the fit. For devices 1 and 2, Q_c is much larger than Q_l for all points. Each color corresponds to a device as in Fig. 3. (b) Temperature dependence of the Q_l for a mode near 4 GHz (mode 3 for Device 1,2 and mode 1 for device 3). Temperatures ≥ 50 mK shown, for thermalization reasons. (c) Lumped circuit model of a resistively shunted Josephson junction. (d) Equivalent series circuit model of a unit cell.

proximate inverse frequency relationship for Devices 1 and 2 (Fig. 4(a)). The observed quality factors are too small in magnitude to be attributed to the external coupling. Furthermore, the frequency dependence of the observed quality factor is opposite from that expected for external coupling. We

therefore conclude that the quality factor is limited by internal loss. The order-of-magnitude change that we observe with increasing frequency is too strong to be associated with dielectric loss^{39,40}. We therefore propose a phenomenological loss model of a resistively shunted Josephson junction that naturally explains the frequency dependence. Qualitatively, the frequency-dependent loss arises from enhanced participation of the shunt resistance as frequency increases (a similar effect was reported in Phan et al²⁰).

The phenomenological loss model includes the Josephson inductance L_J , shunt resistance R_J , and a parasitic capacitance C_0 to the ground. The parallel circuits' impedance can be re-expressed as arising from a series equivalent resistance R_J^* and series equivalent inductance L_J^*

$$R_J^* = \frac{R_J \omega^2 L_J^2}{R_J^2 + \omega^2 L_J^2} \quad (1)$$

$$L_J^* = \frac{L_J R_J^2}{R_J^2 + \omega^2 L_J^2}.$$

In the weak-shunt limit ($R_J > \omega L_J$), relevant here, the shunt resistance is transformed $R_J^* \approx \frac{\omega^2 L_J^2}{R_J}$, whereas $L_J^* \approx L_J$. The series model is equivalent to a lossy transmission line of length $l = Nd$ with N unit cells, resistance per length $R_l^* = R_J^*/d$, and inductance per length $L_l^* = L_J^*/d$. The internal quality factor of the n^{th} mode with frequency $\omega_n = n\omega_0$ is then given by the known formula

$$Q_{i,n} = \frac{n\pi}{2\alpha^* l}, \quad (2)$$

where the attenuation constant is $\alpha^* = R_l^*/(2Z)^{41}$. In terms of the parallel circuit elements, the internal quality factor Q_i as a function of $f_r = \omega_n/(2\pi)$ becomes

$$Q_i = \frac{1}{f_r} \frac{Z R_J}{2N \omega_0 L_J^2}. \quad (3)$$

Equation 3 predicts that Q_i scales as $1/f_r$, as observed in the experiment (most clearly for Devices 1 and 2). Fitting to the data in Fig. 4a along with Z and L values extracted from the finite-element simulations, we extract the device resistance per junction R_J to be 10 k Ω , 11 k Ω , and 3 k Ω for Device 1, 2, and 3. Interestingly, R_J is smaller for Device 3 which has a shorter junction length (400 nm compared with 700 nm), as expected for an intrinsic loss mechanism related to diffusive junctions. Qualitatively, the loss mechanism is reflected in the fact that Device 3 has much higher Q at similar frequencies.

To further explore the loss mechanism in our devices, we studied the temperature dependence of the microwave quality factor for modes of comparable frequency (Fig. 4(b)). Quality factor decreases strongly with temperature, with the longer junctions (Devices 1,2) showing strong temperature dependence below 100 mK. The strong temperature dependence is also suggestive of an intrinsic loss mechanism associated with our long junctions.

Before concluding, we note that Device 3 does not follow the $Q_i \propto 1/f_r$ relation as well as 700 nm devices (Device 1,2)

do. A possible reason for the discrepancy is that the for the first mode of Device 3 Q_i approaches Q_c (Fig 4(a)), whereas for all other modes and devices $Q_i \ll Q_c$. Recall also that the agreement between the EM simulation result and the observed dispersion is worse in Device 3 compared to Device 1 and 2 due to a cooldown-specific microwave problem. Q_i may also have been affected.

III. CONCLUSION

In conclusion, we fabricated Al/InAs superconductors whose characteristic impedance exceeds the resistance quantum. We find linear mode dispersion with no discernible limitations from the single-junction plasma frequency. The observed dispersion matches a model including the periodic inductance of the array and the electromagnetic environment. We further propose resistively shunted junction model that can explain the inverse relation between Q_i and the mode number.

While our experiments do not conclusively determine the microscopic origin of the shunt resistance, we argue that a loss mechanism intrinsic to the junction is plausible. Indeed, our observed quality factors are substantially lower than Al/InAs 2DEG devices with lower junction participation ratios^{17,20,42,43}, pointing to a loss mechanism associated with the junctions. In considering loss mechanisms intrinsic to the junctions, it is important that our devices are in the long-junction limit, $l_J > \xi$ where $\xi \sim 200$ nm is the induced coherence length. We then expect that the junction $I_c R_N$ product is set by the Thouless energy E_{Th} which scales inversely with the square of the junction length. Here, I_c and R_N are the critical current and the normal state resistance of a junction, respectively. An estimate of our Thouless energy implies an R_N order of 0.1 - 1.5 kOhm, compatible with expected long-junction values²⁶. A loss mechanism associated with diffusive junctions is also empirically consistent with the observation that arrays with shorter junctions (Device 3) with proportionately higher critical current and Thouless energy, exhibit higher Q_i . Additionally, we have found that junction loss increases dramatically with temperature, more so for the longer junctions than for the shorter junctions (Fig. 4(b)), consistent with a low Thouless energy $E_{Th} \lesssim k_B T$. Thus, we suspect that the microscopic origin of the resistive shunt is our junction geometry.

To mitigate losses, short junctions could be used as an alternative, provided either the transverse junction dimension is reduced or electrostatic gates are incorporated to maintain sufficiently large Josephson inductance. If the parallel loss channel is reduced, hybrid superinductance would become practically appealing, especially where large plasma frequency or higher operating temperature⁴⁴ is required. At current quality levels, our devices may be competitive for readout of spin²⁷⁻³⁰ and parity qubits³¹⁻³³ at modest frequency < 1 GHz, potentially outperforming dominant coil inductors³⁴ by offering higher quality factor, reduced capacitance, and compact form factor.

IV. ACKNOWLEDGEMENT

This work was funded by the Defense Advanced Research Projects Agency (DARPA) Synthetic Quantum Nanostructures (SynQuaNon) program under Grant Agreement No. HR00112420343 and the NOMIS foundation. Initial device characterizations was performed at the Center for Nanoscale Materials, a U.S. Department of Energy Office of Science User Facility, was supported by the U.S. DOE, Office of Basic Energy Sciences, under Contract No. DE-AC02-06CH11357. This work made use of the shared facilities at the University of Chicago Materials Research Science and Engineering Center, supported by National Science Foundation under award number DMR-2011854.

¹A. Blais, A. L. Grimsom, S. M. Girvin, and A. Wallraff, “Circuit quantum electrodynamics,” *Rev. Mod. Phys.* **93**, 025005 (2021).

²V. E. Manucharyan, J. Koch, L. I. Glazman, and M. H. Devoret, “Fluxonium: Single cooper-pair circuit free of charge offsets,” *Science* **326**, 113–116 (2009).

³L. B. Nguyen, Y.-H. Lin, A. Somoroff, R. Mencia, N. Grabon, and V. E. Manucharyan, “High-coherence fluxonium qubit,” *Physical Review X* **9**, 041041 (2019).

⁴F. Bao, H. Deng, D. Ding, R. Gao, X. Gao, C. Huang, X. Jiang, H.-S. Ku, Z. Li, X. Ma, *et al.*, “Fluxonium: An alternative qubit platform for high-fidelity operations,” *Physical review letters* **129**, 010502 (2022).

⁵L. Ding, M. Hays, Y. Sung, B. Kannan, J. An, A. Di Paolo, A. H. Karamlou, T. M. Hazard, K. Azar, D. K. Kim, *et al.*, “High-fidelity, frequency-flexible two-qubit fluxonium gates with a transmon coupler,” *Physical Review X* **13**, 031035 (2023).

⁶A. Gyenis, P. S. Mundada, A. Di Paolo, T. M. Hazard, X. You, D. I. Schuster, J. Koch, A. Blais, and A. A. Houck, “Experimental realization of a protected superconducting circuit derived from the $0-\pi$ qubit,” *PRX Quantum* **2**, 010339 (2021).

⁷W. Ardati, S. Léger, S. Kumar, V. N. Suresh, D. Nicolas, C. Mori, F. D’Esposito, T. Vakhtel, O. Buisson, Q. Ficheux, *et al.*, “Using bifluxon tunneling to protect the fluxonium qubit,” *Physical Review X* **14**, 041014 (2024).

⁸R. A. Mencia, W.-J. Lin, H. Cho, M. G. Vavilov, and V. E. Manucharyan, “Integer fluxonium qubit,” *PRX Quantum* **5**, 040318 (2024).

⁹N. A. Masluk, I. M. Pop, A. Kamal, Z. K. Minev, and M. H. Devoret, “Microwave characterization of josephson junction arrays: Implementing a low loss superinductance,” *Phys. Rev. Lett.* **109**, 137002 (2012).

¹⁰N. Maleeva, L. Grünhaupt, T. Klein, F. Levy-Bertrand, O. Dupre, M. Calvo, F. Valenti, P. Winkel, F. Friedrich, W. Wernsdorfer, A. V. Ustinov, H. Rotzinger, A. Monfardini, M. V. Fistul, and I. M. Pop, “Circuit quantum electrodynamics of granular aluminum resonators,” *Nature Communications* **9**, 3889 (2018).

¹¹R. Kuzmin, R. Mencia, N. Grabon, N. Mehta, Y.-H. Lin, and V. E. Manucharyan, “Quantum electrodynamics of a superconductor-insulator phase transition,” *Nature Physics* **15**, 930–934 (2019).

¹²S. Mukhopadhyay, J. Senior, J. Saez-Mollejo, D. Puglia, M. Zemlicka, J. M. Fink, and A. P. Higginbotham, “Superconductivity from a melted insulator in josephson junction arrays,” *Nature Physics* **19**, 1630–1635 (2023).

¹³T. Charpentier, D. Perconte, S. Léger, K. R. Amin, F. Blondelle, F. Gay, O. Buisson, L. Ioffe, A. Khvalyuk, I. Poboiko, *et al.*, “First-order quantum breakdown of superconductivity in an amorphous superconductor,” *Nature Physics* **21**, 104–109 (2025).

¹⁴T. Charpentier, A. Khvalyuk, L. Ioffe, M. Feigel’Man, N. Roch, and B. Sacépé, “Universal scaling of microwave dissipation in superconducting circuits,” *arXiv preprint arXiv:2507.08953* (2025).

¹⁵T. W. Larsen, K. D. Petersson, F. Kuemmeth, T. S. Jespersen, P. Krogstrup, J. Nygård, and C. M. Marcus, “Semiconductor-nanowire-based superconducting qubit,” *Physical review letters* **115**, 127001 (2015).

¹⁶F. Luthi, T. Stavenga, O. Enzing, A. Bruno, C. Dickel, N. Langford, M. A. Rol, T. S. Jespersen, J. Nygård, P. Krogstrup, *et al.*, “Evolution of nanowire transmon qubits and their coherence in a magnetic field,” *Physical review letters* **120**, 100502 (2018).

¹⁷L. Casparis, M. R. Connolly, M. Kjaergaard, N. J. Pearson, A. Kringhøj, T. W. Larsen, F. Kuemmeth, T. Wang, C. Thomas, S. Gronin, *et al.*, “Superconducting gatemon qubit based on a proximitized two-dimensional electron gas,” *Nature nanotechnology* **13**, 915–919 (2018).

¹⁸M. Hays, G. de Lange, K. Serniak, D. J. van Woerkom, D. Bouman, P. Krogstrup, J. Nygård, A. Geresdi, and M. H. Devoret, “Direct microwave measurement of andreev-bound-state dynamics in a semiconductor-nanowire josephson junction,” *Phys. Rev. Lett.* **121**, 047001 (2018).

¹⁹L. Tosi, C. Metzger, M. F. Goffman, C. Urbina, H. Pothier, S. Park, A. L. Yeyati, J. Nygård, and P. Krogstrup, “Spin-orbit splitting of andreev states revealed by microwave spectroscopy,” *Phys. Rev. X* **9**, 011010 (2019).

²⁰D. Phan, P. Falthans-Scheinecker, U. Mishra, W. Strickland, D. Langone, J. Shabani, and A. Higginbotham, “Gate-tunable superconductor-semiconductor parametric amplifier,” *Phys. Rev. Appl.* **19**, 064032 (2023).

²¹Z. Hao, T. Shaw, M. Hatipour, W. Strickland, B. Elfeky, D. Langone, J. Shabani, and S. Shankar, “Kerr nonlinearity and parametric amplification with an al-inas superconductor–semiconductor josephson junction,” *Applied Physics Letters* **124** (2024).

²²W. M. Strickland, B. H. Elfeky, L. Baker, A. Maiani, J. Lee, I. Levy, J. Is-sokson, A. Vrajitoarea, and J. Shabani, “Gatemonium: A voltage-tunable fluxonium,” *PRX Quantum* **6**, 010326 (2025).

²³A. Bargerbos, W. Uilhoorn, C.-K. Yang, P. Krogstrup, L. P. Kouwenhoven, G. de Lange, B. van Heck, and A. Kou, “Observation of vanishing charge dispersion of a nearly open superconducting island,” *Phys. Rev. Lett.* **124**, 246802 (2020).

²⁴A. Kringhøj, B. van Heck, T. W. Larsen, O. Erlandsson, D. Sabonis, P. Krogstrup, L. Casparis, K. D. Petersson, and C. M. Marcus, “Suppressed charge dispersion via resonant tunneling in a single-channel transmon,” *Phys. Rev. Lett.* **124**, 246803 (2020).

²⁵M. Vaněvić and Y. V. Nazarov, “Quantum phase slips in superconducting wires with weak inhomogeneities,” *Phys. Rev. Lett.* **108**, 187002 (2012).

²⁶W. Mayer, J. Yuan, K. S. Wickramasinghe, T. Nguyen, M. C. Dartailh, and J. Shabani, “Superconducting proximity effect in epitaxial al-inas heterostructures,” *Applied Physics Letters* **114** (2019).

²⁷D. J. Reilly, C. M. Marcus, M. P. Hanson, and A. C. Gossard, “Fast single-charge sensing with a rf quantum point contact,” *Applied Physics Letters* **91**, 162101 (2007).

²⁸K. D. Petersson, C. G. Smith, D. Anderson, P. Atkinson, G. A. C. Jones, and D. A. Ritchie, “Charge and spin state readout of a double quantum dot coupled to a resonator,” *Nano Letters* **10**, 2789–2793 (2010).

²⁹A. Crippa, R. Ezzouch, A. Aprá, A. Amisse, R. Laviéville, L. Hulin, B. Bertrand, M. Vinet, M. Urdampilleta, T. Meunier, M. Sanquer, X. Jehl, R. Maurand, and S. De Franceschi, “Gate-reflectometry dispersive readout and coherent control of a spin qubit in silicon,” *Nature Communications* **10**, 2776 (2019).

³⁰S. K. Bartee, W. Gilbert, K. Zuo, K. Das, T. Tanttu, C. H. Yang, N. Dummoulin Stuyck, S. J. Pauka, R. Y. Su, W. H. Lim, S. Serrano, C. C. Escott, F. E. Hudson, K. M. Itoh, A. Laucht, A. S. Dzurak, and D. J. Reilly, “Spin-qubit control with a milli-kelvin cmos chip,” *Nature* **643**, 382–387 (2025).

³¹M. Aghaee, A. Alcaraz Ramirez, Z. Alam, R. Ali, M. Andrzejczuk, A. Antipov, M. Astafev, A. Barzegar, B. Bauer, J. Becker, U. K. Bhaskar, A. Bocharov, S. Boddapati, D. Bohn, J. Bommer, L. Bourdet, A. Bousquet, S. Boutin, L. Casparis, B. J. Chapman, S. Chattoor, A. W. Christensen, C. Chua, P. Codd, W. Cole, P. Cooper, F. Corsetti, A. Cui, P. Dalpasso, J. P. Dehollain, G. de Lange, M. de Moor, A. Ekefjärd, T. El Dandachi, J. C. Estrada Saldaña, S. Fallahi, L. Galletti, G. Gardner, D. Governer, F. Griggio, R. Grigoryan, S. Grijalva, S. Gronin, J. Gukelberger, M. Hamdast, F. Hamze, E. B. Hansen, S. Heedt, Z. Heidarnia, J. Herranz Zamorano, S. Ho, L. Holgaard, J. Hornibrook, J. Indrapironkul, H. Ingerslev, L. Ivancevic, T. Jensen, J. Jhoja, J. Jones, K. V. Kalashnikov, R. Kallahe, R. Kalra, F. Karimi, T. Karzig, E. King, M. E. Kloster, C. Knapp, D. Kocan, J. V. Koski, P. Kostamo, M. Kumar, T. Laeven, T. Larsen, J. Lee, K. Lee, G. Leum, K. Li, T. Lindemann, M. Looij, J. Love, M. Lucas, R. Lutchyn, M. H. Madsen, N. Madulid, A. Malmros, M. Manfra, D. Mantri, S. B. Markussen, E. Martinez, M. Mattila, R. McNeil, A. B. Mei, R. V. Mishmash, G. Mohandas, C. Mollgaard, T. Morgan, G. Moussa, C. Nayak, J. H. Nielsen, J. M. Nielsen, W. H. P. Nielsen, B. Nijholt, M. Nystrom, E. O’Farrell, T. Ohki, K. Otani, B. Paquet,

let Wütz, S. Pauka, K. Petersson, L. Petit, D. Pikulin, G. Prawiroatmodjo, F. Preiss, E. Puchol Morejon, M. Rajpalke, C. Ranta, K. Rasmussen, D. Razmadze, O. Reentila, D. J. Reilly, Y. Ren, K. Reneris, R. Rouse, I. Sadovskyy, L. Sainiemi, I. Sanlorenzo, E. Schmidgall, C. Sfiligoj, M. B. Shah, K. Simoes, S. Singh, S. Sinha, T. Soerensen, P. Sohr, T. Stankevic, L. Stek, E. Stuppard, H. Suominen, J. Suter, S. Teicher, N. Thiyagarajah, R. Tholapi, M. Thomas, E. Toomey, J. Tracy, M. Turley, S. Upadhyay, I. Urban, K. Van Hoogdalem, D. J. Van Woerkom, D. V. Viazmitinov, D. Vogel, J. Watson, A. Webster, J. Weston, G. W. Winkler, D. Xu, C. K. Yang, E. Yucelen, R. Zeisel, G. Zheng, J. Zilke, and M. A. Quantum, “Interferometric single-shot parity measurement in inas-al hybrid devices,” *Nature* **638**, 651–655 (2025).

³²N. van Loo, F. Zatelli, G. O. Steffensen, B. Roovers, G. Wang, T. V. Caekenbergh, A. Bordin, D. van Driel, Y. Zhang, W. D. Huisman, G. Badawy, E. P. A. M. Bakkers, G. P. Mazur, R. Aguado, and L. P. Kouwenhoven, “Single-shot parity readout of a minimal kitaev chain,” (2025), arXiv:arXiv:2507.01606 [cond-mat.mes-hall].

³³M. Aghaee, Z. Alam, R. Andersen, M. Andrzejczuk, A. Antipov, M. Astafev, L. Avilovas, A. Azizimanesh, E. Banek, B. Bauer, J. Becker, U. K. Bhaskar, A. G. Boa, S. Boddapati, N. Bohac, J. D. S. Bommer, J. Borovsky, L. Bourdet, S. Boutin, L. Casparis, S. Chakravarthi, H. Chalabi, B. J. Chapman, N. Chatzaras, T.-C. Chien, J. Cho, P. Codd, W. Cole, P. W. Cooper, F. Corsetti, A. Cui, T. E. Dandachi, C. Dinesen, A. Ekefjärd, S. Fallahi, L. Galletti, G. C. Gardner, G. L. Gonzalez, D. Govender, F. Grigorio, R. Grigoryan, S. Grijalva, S. Gronin, J. Gukelberger, M. Hamdast, A. B. Hamida, E. B. Hansen, C. T. Hansen, S. Heedt, S. Ho, L. Holgaard, K. van Hoogdalem, J. Hornibrook, H. Ingerslev, L. Ivancevic, S. Jamo, M. Jantos, T. Jensen, J. S. Jhoja, J. C. Jones, V. Joshi, K. V. Kalashnikov, R. Kallaher, R. Kalra, F. Karimi, T. Karzig, S. Kimes, E. King, M. E. Kloster, C. Knapp, J. V. Koski, P. Kostamo, T. Laeven, J. Lai, G. de Lange, T. W. Larsen, K. Lee, K. Li, G. Li, S. Liang, T. Lindemann, M. Looij, M. Lucas, R. Lutchyn, M. H. Madsen, N. Madulid, M. J. Manfra, L. Manjunath, S. Markussen, E. Martinez, M. Mattila, J. R. Mattinson, R. P. G. McNeil, A. P. Millan, R. V. Mishmash, S. Mittal, C. Møllgaard, M. W. A. de Moor, E. P. Morejon, T. Morgan, G. Moussa, B. P. Nabar, A. Narla, C. Nayak, J. H. Nielsen, W. H. P. Nielsen, F. Nolet, M. J. Nystrom, E. O’Farrell, T. A. Ohki, K. Otani, C. Papon, K. D. Petersson, L. Petit, D. Pikulin, M. Rajpalke, A. A. Ramirez, D. Razmadze, Y. Ren, I. Sadovskyy, L. Sainiemi, J. C. E. Saldaña, I. Sanlorenzo, T. P. dos Santos, S. Schaal, J. Schack, E. R. Schmidgall, C. Sfetsou, C. Sfiligoj, S. Sinha, P. Sohr, T. L. Sørensen, K. Spiegelhauer, T. Stankević, L. J. Stek, P. Strøm-Hansen, H. J. Suominen, J. Suter, S. M. L. Teicher, R. Tholapi, M. Thomas, D. W. Tom, E. Toomey, J. Tracy, M. Turley, M. D. Turner, S. Upadhyay, I. Urban, D. V. Viazmitinov, A. W. Viazmitinova, B. Viegas, D. J. Vogel, J. Watson, A. Webster, J. Weston, T. Williamson, G. W. Winkler, D. J. van Woerkom, B. P. Wuetz, C.-K. Yang, Shang-Jyun, Yu, E. Yucelen, J. H. Zamorano, R. Zeisel, G. Zheng, and A. M. Zimmerman, “Distinct lifetimes for x and z loop measurements in a majorana tetron device,” (2025), arXiv:2507.08795 [cond-mat.mes-hall].

³⁴J. M. Hornibrook, J. I. Colless, A. C. Mahoney, X. G. Croot, S. Blanvillain, H. Lu, A. C. Gossard, and D. J. Reilly, “Frequency multiplexing for readout of spin qubits,” *Applied Physics Letters* **104**, 103108 (2014).

³⁵S. Probst, F. Song, P. A. Bushev, A. V. Ustinov, and M. Weides, “Efficient and robust analysis of complex scattering data under noise in microwave resonators,” *Review of Scientific Instruments* **86** (2015).

³⁶T. Weiβl, B. Küng, É. Dumur, A. K. Feofanov, I. Matei, C. Naud, O. Buisson, F. W. Hekking, and W. Guichard, “Kerr coefficients of plasma resonances in josephson junction chains,” *Physical Review B* **92**, 104508 (2015).

³⁷Y. Krupko, V. Nguyen, T. Weiβl, É. Dumur, J. Puertas, R. Dassonneville, C. Naud, F. Hekking, D. Basko, O. Buisson, *et al.*, “Kerr nonlinearity in a superconducting josephson metamaterial,” *Physical Review B* **98**, 094516 (2018).

³⁸P. Manset, J. Palomo, A. Schmitt, K. Gerashchenko, R. Rousseau, H. Patange, P. Abgrall, E. Flurin, S. Deléglise, T. Jacqmin, *et al.*, “Hyperinductance based on stacked josephson junctions,” arXiv preprint arXiv:2505.02764 (2025).

³⁹J. Gao, *The Physics of Superconducting Microwave Resonators*, Ph.D. thesis, California Institute of Technology, Pasadena, California (2008), ph.D. thesis.

⁴⁰C. Kaiser, S. Skacel, S. Wünsch, R. Dolata, B. Mackrodt, A. Zorin, and M. Siegel, “Measurement of dielectric losses in amorphous thin films at gigahertz frequencies usingsuperconducting resonators,” *Superconductor Science and Technology* **23**, 075008 (2010).

⁴¹D. M. Pozar, *Microwave engineering: theory and techniques* (John wiley & sons, 2021).

⁴²D. Phan, J. Senior, A. Ghazaryan, M. Hatefipour, W. Strickland, J. Shabani, M. Serbyn, and A. P. Higginbotham, “Detecting induced $p\pm ip$ pairing at the al-inas interface with a quantum microwave circuit,” *Physical Review Letters* **128**, 107701 (2022).

⁴³W. M. Strickland, B. H. Elfeky, J. O. Yuan, W. F. Schiela, P. Yu, D. Langone, M. G. Vavilov, V. E. Manucharyan, and J. Shabani, “Superconducting resonators with voltage-controlled frequency and nonlinearity,” *Phys. Rev. Appl.* **19**, 034021 (2023).

⁴⁴S. Telkamp, T. Antonelli, C. Todt, M. Hinderling, M. Coraiola, D. Haxell, S. C. t. Kate, D. Sabonis, P. Zeng, R. Schott, *et al.*, “Development of a nb-based semiconductor-superconductor hybrid 2deg platform,” *Advanced Electronic Materials* **11**, 2400687 (2025).